Proceedings of the Sixteenth International Conference on
Computational Structures Technology
Edited by: P. Iványi, J. Kruis and B.H.V. Topping
Civil-Comp Conferences, Volume 14, Paper 4.3
Civil-Comp Press, Edinburgh, United Kingdom, 2026
ISSN: 2753-3239, doi: 10.4203/ccc.14.4.3

Preliminary Predictions of Progressive Damage in Single-Bolted Pultruded FRP Connections and Comparison with Experiments

A. Rahman, I. Boem and N. Gattesco

Department of Engineering and Architecture, University Trieste, Italy

Abstract

A finite element model was developed in ABAQUS to investigate the nonlinear behaviour and progressive damage of single-bolted double-lap connections in Glass Pultruded Fibre-Reinforced Polymer (PFRP) profiles. The model uses dynamic explicit solver and incorporates the Hashin damage criteria for damage initiation and fracture energy-based formulations for damage evolution and propagation. Nominal mechanical parameters were assumed for the preliminary prediction of the performances of connections under longitudinal tensile loading. The bolt end distance was varied from 2 to 6 times the bolt diameter, to check the possible influence on the capacity and failure modes. According to the same setup, experimental tests were then carried out to obtain empirical evidence and assess the validity of the numerical predictions. The comparison of the results shows good consistency between the numerical and experimental load-displacement capacity of the connections, with good replication of stiffness, peak load, and damage progression in the post-peak stage, till collapse. The model was proved capable to successfully capture key failure modes, namely the shear out and pin bearing, as well as their transition with increasing end distance. The proposed modelling approach thus offers a reliable strategy for predicting the tensile behaviour of PFRP bolted connections and can be extended to multi-bolted configurations without the need for extensive, systemic experimental testing.

Keywords: pultruded profiles, finite element model, explicit solver, Hashin damage criteria, bolted connections, shear out, pin bearing.

1 Introduction

Pultruded Fibre-Reinforced Polymer (PFRP) profiles are nowadays successfully used in the construction of pedestrian bridges, towers, platforms, and other infrastructure systems, particularly for their height strength-to-weight ratio and long-term performance in aggressive and severe environments where conventional materials such as steel or concrete may suffer from durability issues [1,2]. Pultruded profiles are commonly installed using bolted connections, due to their ease of assembly and disassembly, inspection, maintenance, and replacement. Despite these advantages, bolted connections itself introduce localized stress concentrations around the bolts region, which typically govern the strength and failure mode of the structural system.

The behaviour of bolted PFRP connections is influenced by several factors, including material composition (fibres type, amount and orientation), loading direction, and geometric characteristics, namely the PFRP thickness (t) and width (w), as well as the bolt end distance (e), Under in-plane loading conditions, typical failure modes are shear out, pin bearing, net-tension, and splitting (Figure 1). Among these, pin bearing is generally considered a more pseudo-ductile and desirable failure mode, whereas the others are brittle in nature and may lead to sudden collapse without significant warning [3,4].

A comprehensive review of experimental testing on PFRP connections can be found in the authors' previous work [5]. However, experimental studies are often time-consuming and costly, particularly because each pultruded profile may have different material compositions and geometric characteristics, requiring a large number of tests to fully characterize their behaviour. To overcome these limitations, numerical and analytical models have been developed to simulate the behaviour of bolted connections [6–8]. Earliest numerical models primarily focused on linear elastic two or three dimensional analyses. With advancements in computational capabilities, more sophisticated nonlinear models have been introduced to capture damage initiation and progression in composite materials. Commercial finite element software such as ABAQUS [9] and ANSYS provide capabilities for modelling orthotropic elastic behaviour; however, built-in nonlinear damage models are generally restricted to shell (2D geometry) or continuum shell (3D geometry) elements. In particular, the Hashin damage initiation criteria [10], combined with fracture energy-based formulations for damage evolution, is suitable for modelling failure of orthotropic materials such as composite profiles in ABAQUS. In addition to built-in models, several researchers have developed advanced three-dimensional nonlinear material models using user-defined subroutine, such as UMAT (for implicit solvers) and VUMAT (for explicit solvers). While these approaches allow for more accurate representation of complex damage mechanisms, they require significant expertise in programming and implementation, and each model must be individually validated. As a result, such methods are not always readily accessible for general engineering applications. Furthermore, the static general (implicit) solver in ABAQUS often encounters convergence difficulties when simulating highly nonlinear behaviour associated with damage initiation and propagation in composite materials even for the shell and continuum shell elements. These challenges are particularly pronounced in the post-peak regime, where stiffness degradation and localized failure occur and arises convergence problems. To address these limitations, the explicit solver provides an alternative approach, as it does not rely on iterative equilibrium convergence and can effectively handle severe nonlinearities, contact interactions, and progressive damage after the failure load.

In this study, the dynamic explicit solver in ABAQUS is used to investigate the progressive nonlinear behaviour of single-bolted double-lap joints in PFRP profiles, also beyond the peak load. The model incorporates the Hashin damage initiation criteria and a fracture energy-based formulation for damage evolution. Nominal mechanical properties of the PFRP profile are adopted for the simulations, and the end distance is varied from 2*d* to 6*d* to evaluate its influence on mechanical performance and failure modes. Experimental testing is subsequently conducted to check the validity of the numerical model. The paper is structured into two main sections: the first presents the preliminary numerical simulations, while the second provides the experimental results and their comparison with the numerical predictions.

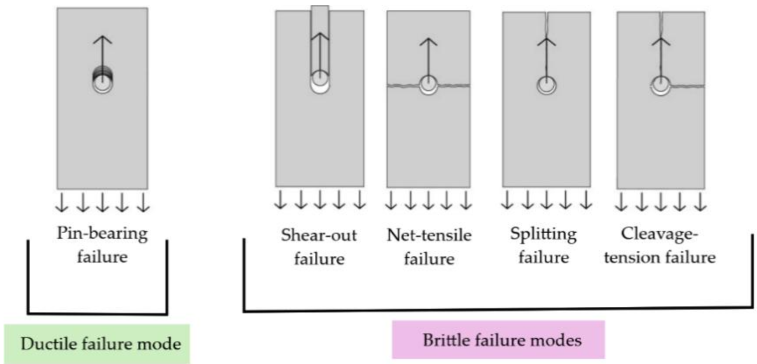

Figure 1. Schematic representation of characteristic failure modes of PFRP bolted connections under longitudinal tensile loading [5]. Reprinted with permission from Rahman, A.; Boem, I.; Gattesco, N., Journal of Composites Science, MDPI, 2025. © under the Creative Commons CC BY license.

2 Numerical Modelling

The finite element model of the single-bolted-double-lap joint for the PFRP profile (Figure 2a,b) was recently developed by the authors [5], using the latest version of ABAQUS (explicit) (2025). The joint configuration comprises of two outer steel plates and an inner pultruded GFRP plate connected through a steel bolt. The X-axis was defined as the longitudinal fibre direction of the PFRP plate, associated with the unidirectional roving, corresponding to the highest elastic modulus. To optimize computational efforts, only one-quarter of the joint was modelled by applying boundary conditions imposed along the plane of symmetry in Y and Z axis. Accordingly, one steel plate was modelled with its full length and thickness but only half of its width, while the PFRP plate was represented with full length but half of its thickness and width. Similarly, only one-quarter of the bolt geometry was incorporated in the model.

Boundary conditions were applied such that the far end of the PFRP plate was fully restricted and fixed in all directions. A displacement increasing linearly along the X-direction was applied to the far end of the steel plate to replicate the experimental loading conditions. A clearance gap of 2.5 mm was introduced among the plates, consistently with the experimental setups used for performing experimental testing.
Further details regarding numerical modelling approach can be found in [5], where the results of an extensive sensitivity analysis and model optimization were also reported and discussed.

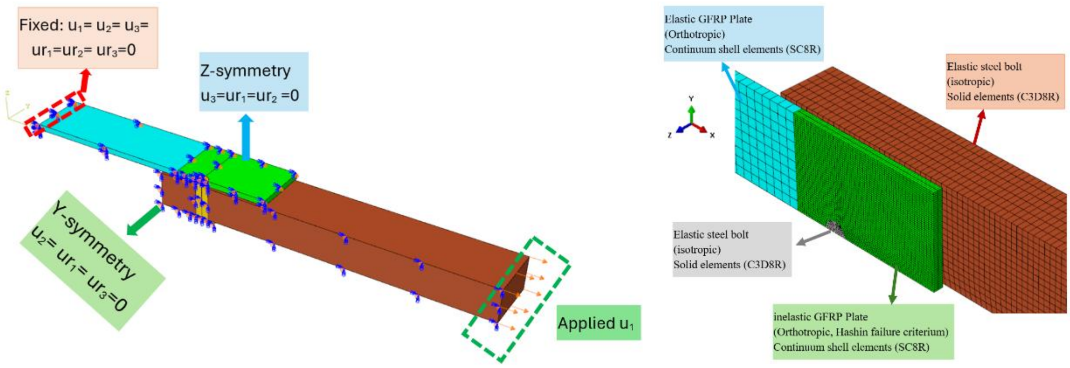

(a) (b)

Figure 2. Schematic representation of the single-bolted-double-lap joint model in ABAQUS: (a) applied boundary conditions; (b) portion of the model showing the meshing scheme.

Eight nodes continuum shell elements with reduced integration (SC8R) were employed to model PFRP plate. To capture localized damage while maintaining computational efficiency, the plate was divided into two regions. The first region was assigned linear elastic properties, while the second region—around the bolt hole, where concentration of stresses and failure are projected—was given nonlinear, damage capable material characteristics. These two regions were connected using tie constraints to ensure continuity. Orthotropic elastic engineering moduli constants were defined for both regions. For the inelastic region, the in-built Hashin damage initiation and evolution criteria which is related to shell and continuum shell elements were applied [10]. Damage initiation was defined using tensile, compressive, and shear strength properties in both the longitudinal (fibre) and transverse (matrix) directions. For damage evolution, fracture energies for tension and compression were specified in both directions.
The PFRP material parameters adopted in the simulations are reported in Table 1: it is observed that for these preliminary predictions, both elastic and strength properties referred to nominal values provided in the product's technical sheet. Differently fracture energies were set up according to the sensitivity analysis carried out in [5].
The steel plates and bolt were represented using eight-node, three-dimensional solid elements with reduced integration (C3D8R), assuming isotropic linear elastic properties with a Young's modulus of 200 GPa and a Poisson's ratio of 0.3.

The use of SC8R elements for the composite and C3D8R elements for the steel enabled accurate modelling of damage mechanisms in the composite while ensuring dependable simulation of the metallic parts.
The general contact algorithm of the explicit solver was employed to model interactions between the bolt and both the steel and PFRP plates. Hard contact was assigned in the normal direction, with a tangential friction coefficient of 0.2, consistent with literature values.
The steel plate was meshed with elements of size 3 × 3 × 10 mm^3, while the bolt used a finer mesh of 1 × 1 × 1 mm^3. For the composite plate, the elastic section was discretized with 5 × 5 × 5 mm^3 elements, whereas the section surrounding the bolt was meshed to 1 × 1 × 2.5 mm^3, including 2.5 mm in the thickness direction.
The simulations were performed using the explicit solver with a dynamic procedure. The displacement applied to the steel plate was ramped gradually to minimize dynamic effects, ensuring that the kinetic energy remained negligible compared to the input energy. Mass scaling with a target increment of 5×10^{-7} was used to reduce computational time without affecting accuracy, decreasing the simulation duration from approximately 24–42 hours to 2–6 hours on an 8-core machine [5].

Property	**Value**
Elastic properties	
Longitudinal Young's Modulus (MPa)	27000
Transverse Young's Modulus (MPa)	7000
In-plane Shear Modulus (MPa)	4000
Interlaminar shear modulus (MPa)	4000
Poisson ratio (υ_{12})	0.3
Poisson ratio (υ_{23})	0.3
Strengths	
Longitudinal Tensile Strength (MPa)	427.9
Longitudinal Compressive Strength (MPa)	330.6
Transverse Tensile Strength (MPa)	118.8
Transverse Compressive Strength (MPa)	51.3
In-plane Shear Strength (MPa)	30.0
Interlaminar shear strength (MPa)	18.5
Fracture energies	
Longitudinal Tensile Fracture Energy (LT-FE) (MPa.mm)	100
Longitudinal Compressive Fracture Energy (LC-FE) (MPa.mm)	150
Transverse Tensile Fracture Energy (TT-FE) (MPa.mm)	30
Transverse Compressive Fracture Energy (TC-FE) (MPa.mm)	20

Table 1. Mechanical parameters of the PFRP profile

The behaviour of single-bolted connections with a PFRP plate thickness t=10 mm, bolt diameter d=12 mm, and bolt end distances e ranging from 2d to 6d was firstly simulated. The corresponding capacity curves of the connections, presented in Figure 3, are obtained by plotting the longitudinal tensile load and corresponding relative displacement between the PFRP and the steel plate.

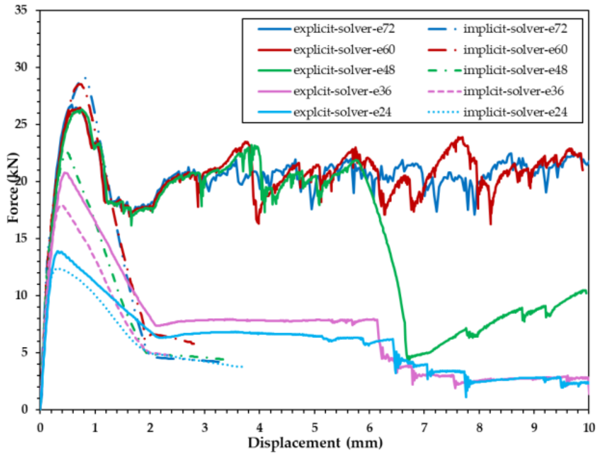

Figure 3. Numerical capacity curve on the single-bolted PFRP connections, varying the end distance from 2*d* (e24) to 6*d* (e60). Solid and dashed lines refer to explicit and implicit analysis, respectively).

Looking at the curves, it is firstly observed that the initial stiffness of the connections is not appreciably influenced by the bolt end distance, while the capacity of the connection increases with *e*, moving from 2*d* to 4*d*. Conversely, a just very slightly higher resistance emerges from the 5*d* and 6*d* configurations, as compared to 4*d*. The post-peak trend of the curves reproduces a brittle behaviour, for *e* = 2*d* to 3*d*, reflecting a shear out dominated failure. Differently, mode ductile behaviour emerged from the 4*d* to 6*d* connections, accordingly to the occurrence of pin bearing mechanism; however, as the displacement increases, the effective end distance progressively reduces and the shear out failure then occurs, then leading to the abrupt load drop down. The increase of the end distance beyond 4*d* delays the onset of shear-out failure, shifting it to a later stage in the load–displacement response.

The numerical results demonstrate that both brittle shear out and pseudo-ductile pin bearing failures can be captured by the model without any convergence issue. In contrast, simulations performed using the static implicit solver exhibit significant convergence difficulties beyond the peak load, as also shown in dashed lines in Figure 3, for comparison. In fact, during the post-peak regime, the implicit solver requires progressively smaller time increments—often reaching values as low as 1×10^{-9}—which can cause the analysis to terminate prematurely. As a result, the implicit solver fails to capture the complete post-peak response and is unable to simulate certain failure modes, such as pin bearing mechanism.

These limitations arise because the implicit solver relies on iterative equilibrium convergence at each load step. While this approach is efficient for linear or mildly nonlinear problems, it becomes unreliable when significant stiffness degradation, crack propagation, or localized damage occurs. In such cases, the loss of stiffness during post-peak behaviour leads to convergence failure. Conversely, the explicit solver integrates the equations of motion over very small-time increments, enabling it to effectively capture the full load–displacement response, including peak load, post-peak softening, and progressive failure mechanisms. This capability is particularly important for composite connections, where failure typically initiates in localized regions around the bolt and subsequently propagates, potentially leading to partial separation of the material. The explicit formulation ensures that these complex damage processes are simulated accurately without the need for artificial stabilization techniques. Although the explicit method is computationally more demanding, its robustness in handling severe nonlinearities, contact interactions, and damage evolution justifies its use in the present study and in future steps of this research, where multiple-bolt connections will be addressed.

The damage patterns at various relative displacements, obtained for connections with *e*=2*d* to 6*d* are presented in Figure 4a–e. The damage index, ranging from 0 (undamaged) to 1 (fully damaged), clearly illustrates the progressive evolution of shear damage.
In particular, for smaller end distances (*e*=2*d* and 3*d*) as shown in Figure 4a-b, the numerical simulations indicate that shear damage initiates along the shear plane near the bolt hole at displacement of 0.09 mm and progressively propagates towards the plate edge along the longitudinal loading direction, ultimately leading to complete shear out failure. The shear damage along the whole end distance in case of *e*=2*d* and 3*d* ends at relative displacement of 0.51mm and 0.62 mm, respectively, where the shear out failure occurs. In these cases, compressive damage around the hole remains negligible prior to shear out failure.
For larger end distances, particularly at *e*=4*d, 5d* and 6*d*, as shown in Figure 4c-e, the numerical model captures a more complex failure mechanism. Initial shear damage develops around the bolt hole similar to *e*=2*d* and 3*d* at displacement of 0.09 mm, leading to a gradual reduction in stiffness, followed by compressive damage, that started in the longitudinal fibre direction around the hole, at relative displacement of approximately 0.39 mm. The elements of PFRP plate around the hole on compressed edge fully damaged by compression action of the bolt at relative displacement of 0.80 mm in all the three cases, where the pin bearing failure occurred. As loading progresses, this is followed by the development of complete shear damage along the shear plane in case of *e*=4*d*, ultimately resulting in final shear out failure at displacement of 6.10 mm. Conversely, in case of *e*=5*d* and 6*d,* the shear damage along the end distance does not complete till relative displacement of 10 mm and expected to occur, eventually, at a larger displacement. This sequence of damage evolution, demonstrating the capability of the model to capture first the pseudo-ductile pin bearing failure followed by the brittle shear out failure.

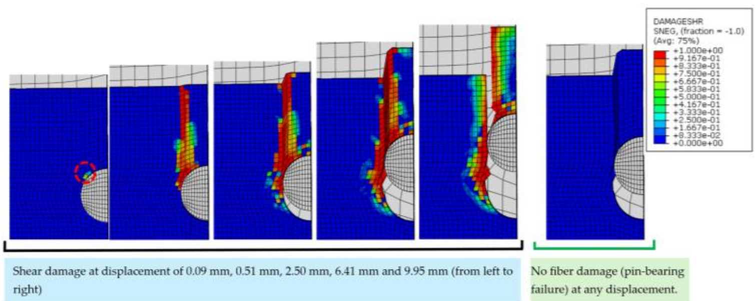

(a)

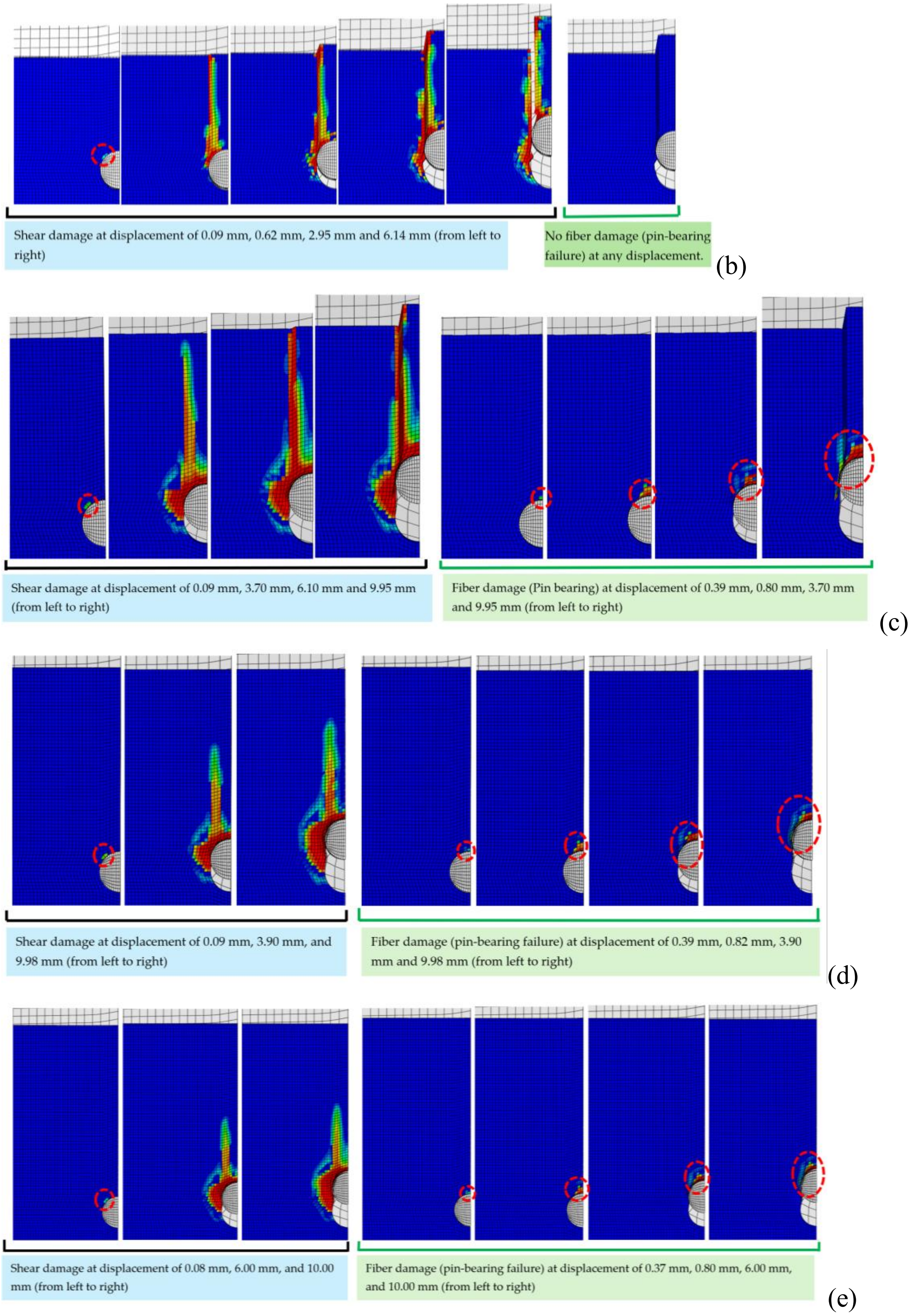

Figure 4. Numerical damage patterns for PFRP bolted connections with bolt end distance of: (a) *e*=2*d*, (b) *e*=3*d*, (c) *e*=4*d*, and (d) *e*=5*d* (e) *e*=6*d*

3 Experimental Tests and Comparison

The preliminary numerical results are compared with experimental tests carried out by the authors for single-bolted connections, considering the same configurations.
The 10 mm thick PFRP material consisted of E-glass fibres embedded in an isophthalic polyester resin, with a fibre weight fraction of 68%. The laminate includes 90° fabric layers with a total areal weight of 2658 g/m², along with 900 g/m² of continuous filament mats to enhance the transverse mechanical properties.
The experimental arrangement, illustrated in Figure 5, replicated the same setup of the numerical model, with the PFRP plate sandwiched between the two steel plates. The bolt was positioned through the three aligned plates, into calibrated holes, creating two shear planes. A small gap (2.5 mm) was maintained between the PFRP profile and each steel plate, ensuring a proper alignment of the specimen and preventing unintended confinement of PFRP during loading. The steel plates were connected to the top loading cell of the testing machine (200 kN), enabling accurate measurement of the applied tensile load. The assembly was suspended from the crossbeam of a steel portal frame anchored to the laboratory floor. The bottom end of the PFRP specimen was clamped between two steel plates, which were connected to the electromechanical actuator fixed to the laboratory floor, and through which the controlled tensile displacement was applied. This loading arrangement allows the assembly to experience a uniaxial tensile force.

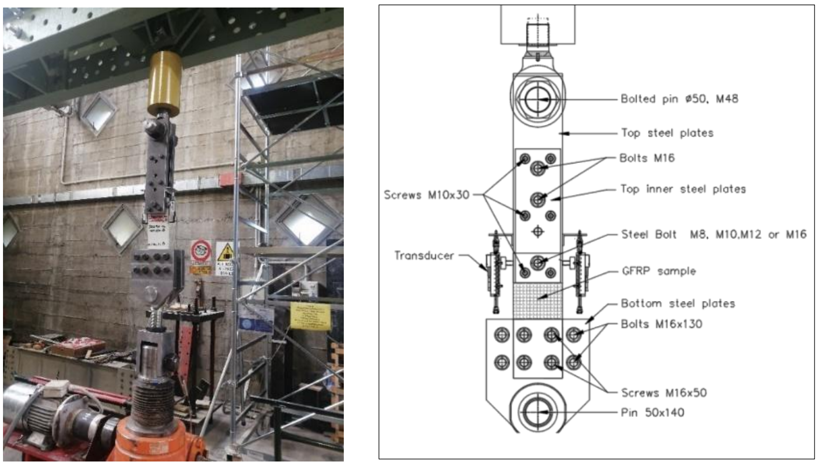

(a) (b)

Figure 5. The experimental setup for testing single-bolted PFRP connections: (a) general view and (b) schematization.

Two displacement transducers (LVDTs, stroke length 50 mm) were employed to monitor the relative displacement between the inner PFRP plate and the outer steel plates: one extremity of the transducers was fixed on the two steel plates (one transducer at each lateral side); the other extremity was fixed on the inner PFRP plate, aligned with the bolt hole centreline. The base measurement length was 60 mm. By averaging the readings from both transducers, any minor rotation of the specimen was minimized, ensuring that the measured deformation reflects the true local response of the connection. The testing apparatus was designed to be sufficiently rigid, allowing displacement-controlled tests to be performed without parasitic effects due to elastic draw-back effects. The applied loading rate ranged between 1 and 2 mm/min (mean displacement monitored by the two transducers), to maintain the quasi-static loading condition.

For each configuration, from *e*=2*d* to *e*=5*d*, three specimens were generally tested; the resulting capacity curves are compared with the corresponding numerical predictions in Figure 6.

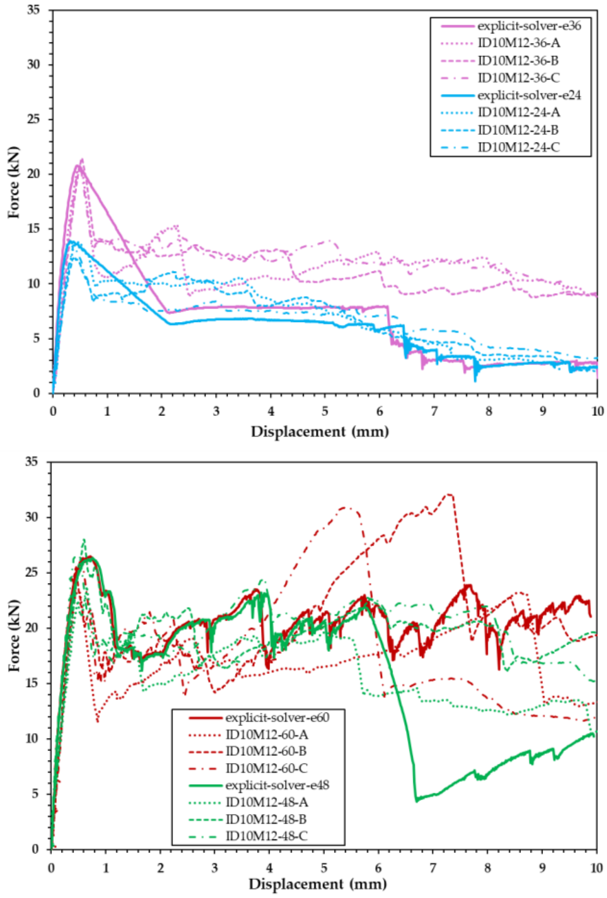

Figure 6. Comparison of experimental and numerical capacity curves for 10 mm thick PFRP bolted connections with end distance of : (a) *e*=2*d* and 3*d*, (b) *e*=4*d* and 5*d*.

For connections with *e*=2*d*, and 3*d*, the numerical capacity curves obtained using the explicit solver show very good agreement with the experimental results, consistently capturing the initial elastic response, peak load, and subsequent post-peak behaviour. In particular, the sudden load drop observed in the experiments is also reproduced in the numerical simulations, corresponding to shear out failure occurring immediately after the peak load.
For the largest end distances (*e*=4*d* and 5*d*), the numerical models successfully capture the pin bearing dominated failure observed experimentally. In case of *e*=4*d*, proceeded by shear out failure at a later stage, demonstrating consistent behaviours between simulations and tests. The numerical model successfully reflects these transitional

behaviours, where the failure mode shifts from shear out to pin bearing with increasing end distance. Actually, a hardening phase was observed in the experimental tests for the *5d* specimens, which preceded the shear-out failure. This is likely related to a local passive confinement effect of the steel plates on the PFRP, once they came into contact due to PFRP expansive damage and spalling around the hole. This aspect was not considered in the numerical model.

The final damage patterns obtained from experimental testing for specimens with *e*= 2*d* to 5*d* are reported in Figure 7a–d and can be directly compared with numerical damage pattern plotted in Figure 4. For smaller end distances (*e*=2*d* and 3*d*), good agreement is observed between the experimental and numerical results, with both exhibiting dominant shear out failure. For larger end distances, specifically at *e*=4*d* and 5*d*, the experiments show pin-bearing failure first, followed by shear out failure only at later stage, consistently with the numerical outcomes. Actually, in case of *e*=5*d*, the numerical model was simulated till a relative displacement of 10 mm where pin-bearing only occurred, while the complete shear out failure may occur at larger displacement beyond 10 mm.

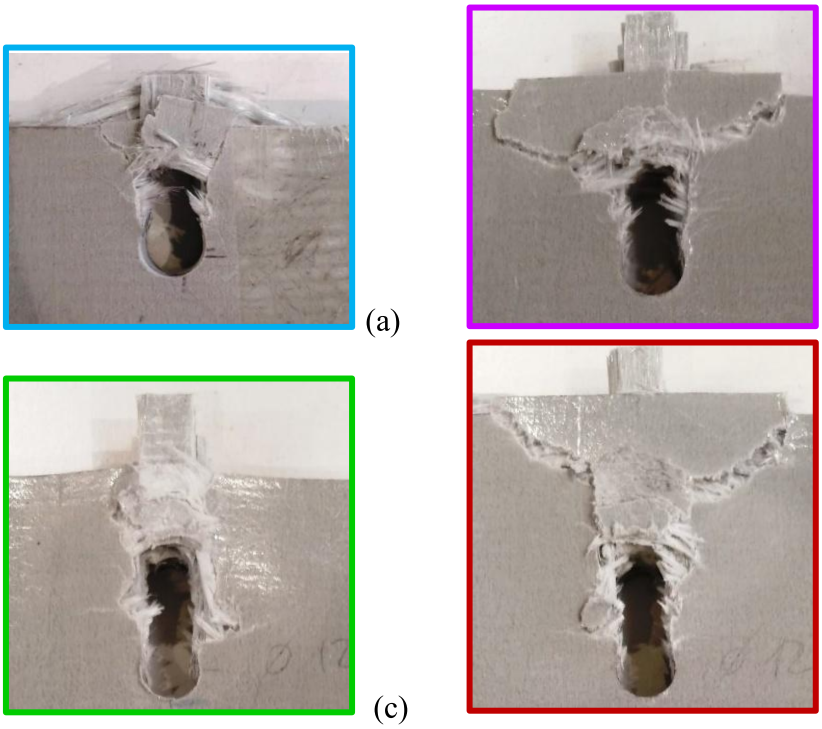
(a) (b) (c) (d)

Figure 7. Final experimental damage patterns for 10 mm thick PFRP bolted connections with end distance of : (a) *e*=2*d*, (b) *e*=3*d*; (c) *e*=4*d*, and (d) *e*=5*d*.

Overall, the comparison with numerical model demonstrates that the explicit numerical model is capable of correctly reproducing the key damage mechanisms and failure patterns across different end distances. It should be noted, in particular, that the preliminary numerical simulations are based on the nominal mechanical parameters of PFRP provided in the product technical sheet.

Specific experimental mechanical characterization tests of PFRP are currently in progress, in order to accurately calibrate such parameters and, consequently, improve the accuracy of the numerical results.

4 Conclusions

A comprehensive numerical and experimental study was conducted to investigate the behaviour of single-bolted double-lap PFRP-steel connections. The developed ABAQUS/Explicit model, incorporating continuum shell elements and Hashin damage initiation criteria and fracture energies-based criteria for damage evolution and progression, demonstrated strong capability in capturing the full load–displacement response, including post-peak softening and progressive failure. The preliminary numerical results closely matched the experimental observations for all configurations, successfully capturing both shear out and pin bearing failure modes, as well as the shift between them with increasing the bolt end distance. The explicit solver proved essential for handling severe nonlinearities and damage evolution, where the implicit approach was unable to converge beyond peak load. Overall, the validated numerical model provides an effective tool for analysing the structural performance of PFRP bolted connections and can support future design and optimisation of composite structural systems, also considering multiple-bolt configurations.

Acknowledgements

The financial support of the Italian Ministry of University and Research (MUR) and of Fibre-Net industry S.p.A are gratefully acknowledged.

References

1. Hollaway, L.C. A Review of the Present and Future Utilisation of FRP Composites in the Civil Infrastructure with Reference to Their Important In-Service Properties. *Constr. Build. Mater.* **2010**, *24*, 2419–2445, doi:10.1016/j.conbuildmat.2010.04.062.
2. Qureshi, J. A Review of Fibre Reinforced Polymer Structures. *Fibers* **2022**, *10*, 27, doi:10.3390/fib10030027.
3. El-Sisi, A.; Hassanin, A.; Alsharari, F.; Galustanian, N.; Salim, H. Failure Behavior of Composite Bolted Joints: Review. *CivilEng* **2022**, *3*, 1061–1076, doi:10.3390/civileng3040060.
4. Tajeuna, T.A.; Légeron, F.; Langlois, S.; Labossière, P.; Demers, M. Effect of Geometric Parameters on the Behavior of Bolted GFRP Pultruded Plates. *J. Compos. Mater.* **2016**, *50*, 3731–3749, doi:10.1177/0021998315625101.
5. Rahman, A.; Boem, I.; Gattesco, N. Numerical Study on the Performance and Failure Modes of Bolted Connections in Pultruded-Fibre-Reinforced Polymer (PFRP) Profiles. *Journal of Composites Science* **2025**, *9*, 492, doi:10.3390/jcs9090492.

6. Turvey, G.J.; Wang, P. An FE Analysis of the Stresses in Pultruded GRP Single-Bolt Tension Joints and Their Implications for Joint Design. *Comput. Struct.* **2008**, *86*, 1014–1021, doi:10.1016/j.compstruc.2007.04.026.
7. Arruda, M.R.T.; Trombini, M.; Pagani, A. Implicit to Explicit Algorithm for ABAQUS Standard User-Subroutine UMAT for a 3D Hashin-Based Orthotropic Damage Model. *Applied Sciences* **2023**, *13*, 1155.
8. Du, A.; Liu, Y.; Xin, H.; Zuo, Y. Progressive Damage Analysis of PFRP Double-Lap Bolted Joints Using Explicit Finite Element Method. *Compos. Struct.* **2016**, *152*, 860–869, doi:10.1016/j.compstruct.2016.06.028.
9. Börgesson, L. Abaqus. In *Developments in geotechnical engineering*; Elsevier, 1996; Vol. 79, pp. 565–570 ISBN 0165-1250.
10. Hashin, Z. Failure Criteria for Unidirectional Fiber Composites. **1980**.